# Enhanced photocatalytic activity of In-$TiO_2$ supported on HZSM-5 zeolite

WENJIE ZHANG*, JIAO YANG, XIAOBEI PEI
*School of Environmental and Chemical Engineering, Shenyang Ligong University, Shenyang 110159, China*

Indium doped $TiO_2$ photocatalyst was supported on HZSM-5 by sol-gel method. The diffraction patterns of the supported In-$TiO_2$($x$)/HZSM-5 samples can be distinguished as the combination of anatase $TiO_2$ and HZSM-5 zeolite. The typical FT-IR absorptions from $TiO_2$ and HZSM-5 indicate the physical loading of In-$TiO_2$ on the surface of HZSM-5. The bandgap energy of In-$TiO_2$ is 2.74 eV. The increase of HZSM-5 content leads to a slight blue shift of the absorption edge. Specific surface area of In-$TiO_2$($x$)/HZSM-5 is much larger than that of In-$TiO_2$. The In-$TiO_2$(50%)/HZSM-5 sample has the optimal activity on photocatalytic degradation of methyl orange.

(Received February 14, 2017; accepted April 5, 2018)

*Keywords:* $TiO_2$, Indium, Photocatalytic, HZSM-5, Methyl orange

## 1. Introduction

Organic pollutants in the wastewater have to be treated before discharging into the aquatic system. As one of the advanced oxidation methods in wastewater treatment, photocatalytic technique has been studied for nearly half a century [1-3]. One of the research focuses in this field is to develop materials with powerful activity on photocatalytic degradation of organic pollutants. $TiO_2$ is the most studied material for this purpose in the past decades [4-6]. However, pure $TiO_2$ is not satisfactory due to many of its defects such as large bandgap and high recombination rate of charge carriers. Normally, modification on $TiO_2$ is necessary to improve its activity [7,8].

Metal ion doping in $TiO_2$ is usually applied as a major modification method in order to extend the lifetime of photogenerated electron-hole pairs. Combination of the charge carriers can be retarded in the doped $TiO_2$, so that photocatalytic activity of the material is promoted [9-11]. Many elements can be used as effective dopants in $TiO_2$-based materials. Gonzalez et al. [12] prepared $In_2O_3$-$TiO_2$ material using sol-gel and impregnation methods. Wang et al. [13] prepared In-doped $TiO_2$ by sol-gel method using titanium tetrabutoxide and indium chloride as precursors.

Moreover, powder material is not usually applied in wastewater treatment due to the difficulty in separating photocatalyst and the treated water. Photocatalyst can be loaded on some kinds of supports to avoid this obstacle. Zeolite is one of the good choices in selecting support for photocatalyst. The superiorities of using zeolite as the support are not only the high specific surface, but also the ability in controlling charge transfer [14]. We have previously used HZSM-5 to support $TiO_2$ with enhancing activity [15,16].

The combination of supporting and metal ion doping is very interesting since not only the material can be easily recycled after treatment, but also the activity of the doped $TiO_2$ can be enhanced after loading on HZSM-5. The preparation of indium doped $TiO_2$ photocatalyst supported on HZSM-5 by sol-gel method was studied in this work. The effects of In-$TiO_2$ loading content on the enhanced activity of In-$TiO_2$($x$)/HZSM-5 photocatalyst were investigated.

## 2. Experimental

### 2.1. Synthesis of In-$TiO_2$ supported on HZSM-5

Indium doped $TiO_2$ was synthesized by sol-gel method. Two solutions were mixed to prepare the sol-gel precursor. One solution was composed of anhydrous ethanol and distilled water. The other solution was made from $In(NO_3)_3$, anhydrous ethanol, tetrabutyl titanate and concentrated hydrochloric acid. HZSM-5 was added into the precursor under stirring. The mixture was stirred for 1 h until the gel formed. The gel was aged at ambient temperature for 12 h, followed by drying at 80 $^oC$ in the furnace. The solid was ground into fine powders and transferred into an oven. Heating rate of the oven was 5 $^oC$ /min. The powders were calcined at 400 $^oC$ for 2 h. The product was ground again and marked as In-$TiO_2$($x$)/HZSM-5, where $x$ represents the loading content of In-$TiO_2$ in the composite. The indium doping ratio $n$(In)/$n$(Ti) is 3% in all the samples.

### 2.2. Characterization of photocatalysts

A D8 X-ray diffractometer was used to measure

diffraction patterns of the materials, using monochromatized Cu *Kα* at λ=1.5416Å. The surface morphology was observed by QUANTA 250 scanning electron microscope at an accelerating voltage of 30 kV. A thin layer of gold was coated on the samples to avoid charging. Infrared absorption spectra were recorded by a Frontier FT-IR/FIR spectrometer in the wavenumber between 50 $cm^{-1}$ and 4000 $cm^{-1}$. UV-Vis diffuse reflectance spectra were recorded by LAMBDA 35 UV-Vis spectrometer equipped with an integrating sphere. The spectra were measured using $BaSO_4$ as a reference. Specific surface area of the materials was measured through $N_2$ adsorption-desorption by an F-sorb 3400 analyzer.

### 2.3. Decoloration of methyl orange

Decoloration of methyl orange (MO) was measured to study the activity of the materials. A 100 mL quartz beaker and a 20 W UV-light lamp irradiating at 253.7 nm were set up as the lap-scale reactor. 15 mg $TiO_2$ and 50 mL of 10 mg/L MO solution were used in each experiment. In prior to turn on the light, the suspension was ensured adsorption-desorption equilibrium after stirring in the dark for 60 min. Adsorption percent of MO on the photocatalyst was measured at this moment. The average irradiation intensity was 1300 $\mu W/cm^2$, measured on the surface of the suspension using an actinometer. The irradiation time in the subsequent experiments was set to 30 min except for the prolonged time reaction. Absorbance of the solution was measured by a 721E spectrophotometer at the maximum absorption wavelength of MO, i.e. 466 nm. MO concentration was calculated according to Lambert-Beer theory.

## 3. Results and discussion

Fig. 1 shows XRD patterns of HZSM-5 and In-$TiO_2$(*x*)/HZSM-5. Zeolite HZSM-5 ($SiO_2/Al_2O_3$=50) was obtained from Nankai Catalyst Corporation, China. Chemical composition of the zeolite is 2.1-2.3% $Na_2O$, 2.3-2.5% $Al_2O_3$, and 86.0-87.0% $SiO_2$. HZSM-5 is composed of tetrahedral Si-O and Al-O skeletons. The diffraction pattern of HZSM-5 represents the composition of this zeolite [17,18]. Pure In-$TiO_2$ is composed of anatase phase $TiO_2$ with the preferred orientation at the (101) plane. The diffraction patterns of the supported In-$TiO_2$(*x*)/HZSM-5 samples can be distinguished as the combination of anatase $TiO_2$ and HZSM-5 zeolite. Diffraction intensities of each constituent depend on the weight content in the composite. Other phases of $TiO_2$ such as rutile phase are not produced in the samples. The diffraction peak of the anatase (101) plane is used to calculate crystallite size, according to Scherrer formular. The crystallite sizes of In-$TiO_2$, In-$TiO_2$(50%)/HZSM-5 and In-$TiO_2$(90%)/HZSM-5 are 8.7, 7.3 and 7.2 nm, respectively. The distribution of $TiO_2$ on the surface of HZSM-5 particles is responsible for the restrained crystal growing [15,16].

Surface morphologies of the In-$TiO_2$ and In-$TiO_2$(*x*)/HZSM-5 samples are presented in the SEM images in Fig. 2. The pure In-$TiO_2$ sample is composed of irregular shaped particles in the size as large as several micrometers, indicating the strong aggregation effect during synthesizing process. There are also many small particles amog the large ones due to grinding of the material after calcination. The HZSM-5 particles normally have regular shape in the size of 2×3×6 $\mu m^3$. The HZSM-5 particles are coated with a layer of $TiO_2$ in the In-$TiO_2$(*x*)/HZSM-5 composite. As can be seen from the figure, some HZSM-5 particles can still be distinguished in the images of the supported samples.

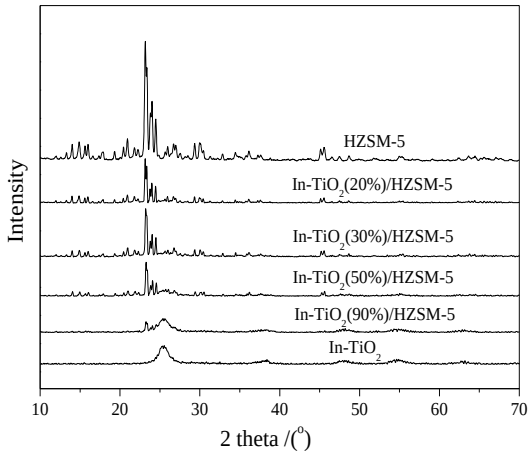


*Fig. 1. XRD patterns of HZSM-5 and In-$TiO_2$(x)/HZSM-5*

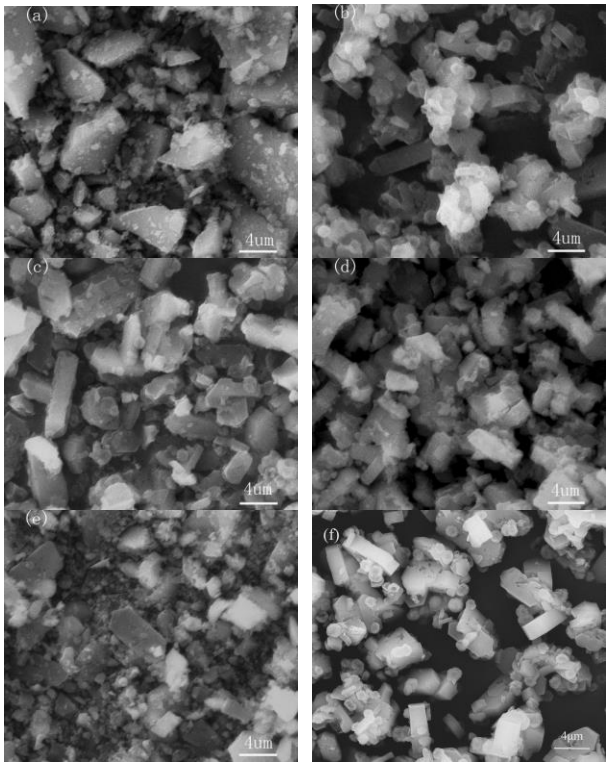


*Fig. 2. SEM images of In-$TiO_2$ and In-$TiO_2$(x)/HZSM-5 (a) In-$TiO_2$, (b) In-$TiO_2$(20%)/HZSM-5, (c) In-$TiO_2$(30%)/HZSM-5, (d) In-$TiO_2$(50%)/HZSM-5, (e) In-$TiO_2$(90%)/HZSM-5, (f) HZSM-5*

Fig. 3 shows FT-IR spectra of In-$TiO_2$(*x*)/HZSM-5 with different In-$TiO_2$ loading contents. Both the typical absorptions from $TiO_2$ and HZSM-5 can be found in the spectra. The broad absorption peak between 400 and 500 $cm^{-1}$ in the FT-IR spectrum of unloaded In-$TiO_2$ is attributed to bending vibration of Ti-O-Ti in anatase $TiO_2$. This absorption still occurs in the spectra of the supported samples. The bending vibration peak of tetrahedral $Al(Si)O_4$ at 452 $cm^{-1}$ overlaps with the above-mentioned bending vibration peak of Ti-O-Ti. The absorption at 547 $cm^{-1}$ is due to the penta-ring vibration in HZSM-5, and the absorption at 745 $cm^{-1}$ is related to symmetric stretching vibration of Al(Si)-O-Al(Si) [19]. The anti-symmetric stretching vibration of Al(Si)-O-Al(Si) has a strong absorption around 1073 $cm^{-1}$ [20]. The absorption intensities of the functional groups in HZSM-5 are in accordance to the content of the zeolite in the composite. It seems that there is no noticeable interaction between In-$TiO_2$ and HZSM-5. The typical absorption belonging to Ti-O-Si is not found in the spectra [21]. In-$TiO_2$ is physically loaded on the surface of HZSM-5 particles. Bending and stretching vibrations of O-H appear at 1630 $cm^{-1}$ and 3446 $cm^{-1}$, indicating the adsorbed water on the surface [22].

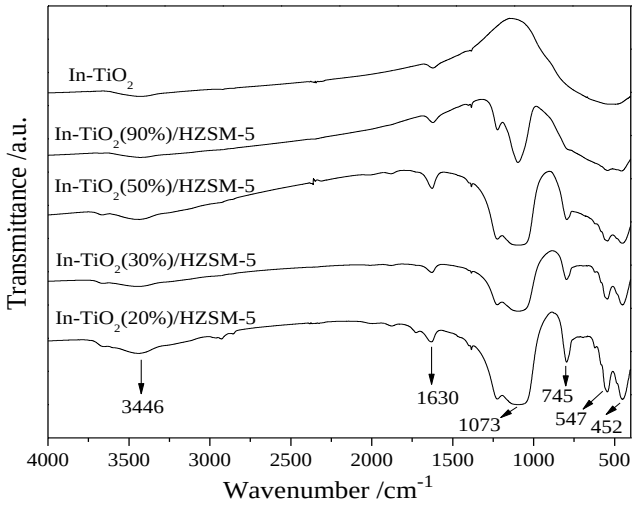


*Fig. 3. FT-IR spectra of In-$TiO_2$(x)/HZSM-5 with different In-$TiO_2$ loading contents*

UV-Vis diffuse reflectance spectra of In-$TiO_2$(*x*)/HZSM-5 are shown in Fig. 4 to show the effect of loading content on bandgap energy. The bandgap energy of the sample is calculated using Kubelka-Munk theory [23] through the formula $(\alpha hv) = A(hv-Eg)^n$, where $\alpha$, $h$, $v$, $A$ and $Eg$ are the absorption coefficient, Planck constant, light frequency, proportionality constant and bandgap energy, respectively [24]. All the samples have strong absorption in the UV region. The bandgap energy of In-$TiO_2$ is 2.74 eV. The samples containing 20%, 30%, 50% and 90% In-$TiO_2$ have the bandgap energies of 2.91, 2.87, 2.78 and 2.76 eV, respectively. The increase of HZSM-5 content leads to a slight blue shift of the absorption edge since the bandgap energy of HZSM-5 is much larger than that of bulk In-$TiO_2$.

Table 1 gives the specific surface areas of In-$TiO_2$(*x*)/HZSM-5 and HZSM-5. HZSM-5 is a kind of zeolite with highly ordered porous structure. The BET surface area of HZSM-5 is as high as 338 $m^2/g$. The unloaded In-$TiO_2$ has a surface area of 96.9 $m^2/g$. The In-$TiO_2$(*x*)/HZSM-5 is the composite of In-$TiO_2$ and HZSM-5. BET surface area of the In-$TiO_2$(*x*)/HZSM-5 sample increases with rising HZSM-5 content. Most of the surface area is provided by the HZSM-5 particles. Meanwhile, partial surface of HZSM-5 particles is covered by In-$TiO_2$.

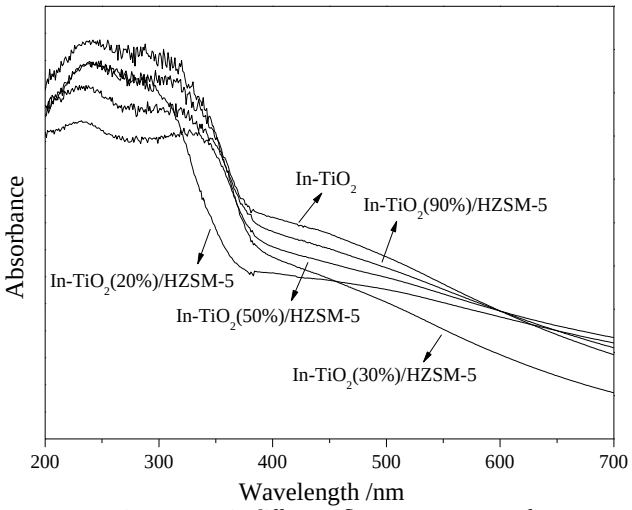


*Fig. 4. UV-Vis diffuse reflectance spectra of In-$TiO_2$(x)/HZSM-5*

*Table 1. Specific surface area of In-$TiO_2$(x)/HZSM-5 and HZSM-5*

| Loading content | 20% | 30% | 50% | 90% | In-$TiO_2$ | HZSM-5 |
|---|---|---|---|---|---|---|
| $S_{BET}$ /$m^2/g$ | 253.3 | 243.8 | 175.9 | 139.6 | 96.9 | 338 |

Indium doping can improve photocatalytic activity of $TiO_2$. The optimal In doping content is 3%, as indicated in our previous work [25]. Fig. 5(a) compares the adsorption and photocatalytic degradation of methyl orange on In-$TiO_2$(*x*)/HZSM-5. Methyl orange can be removed from the solution by both adsorption and photocatalytic degradation processes. The unloaded In-$TiO_2$ has the maximum capacity on adsorption of the dye, while adsorption efficiency decreases after supporting the photocatalyst on the surface of HZSM-5 particles. On the other hand, photocatalytic degradation efficiency as a factor of In-$TiO_2$ loading content has a different trend. The In-$TiO_2$(50%)/HZSM-5 sample has the optimal activity on photocatalytic degradation of methyl orange. 60% of the initial methyl orange molecules in the solution is degraded after 30 min of UV light irradiation.

Both the adsorption capacity and photocatalytic activity depend on the surface characters of the materials, such as specific surface area, surface groups and porosity.

Adsorption of the dye can remove the organic substance from the solution, but it cannot lead to decomposition of the hazardous pollutant. Photocatalytic oxidation can result in overall degradation of organic pollutants in aquatic system. Fig. 5(b) shows UV-Vis absorption spectra of methyl orange solution in presence of In-$TiO_2$(50%)/HZSM-5 during illumination. Methyl orange solution has absorptions in both visible and UV regions. The orange color of the solution comes from the conjugated chromophore in methyl orange molecule. The chromophore group has the maximum absorption intensity at 466 nm in the visible region. The removal of the dye from solution is recorded by measuring the absorption intensity at this wavelength. As can be seen from the figure, nearly all the absorptions in the visible region disappear after 80 min of irradiation. The methyl orange molecules are almost decomposed at this time.

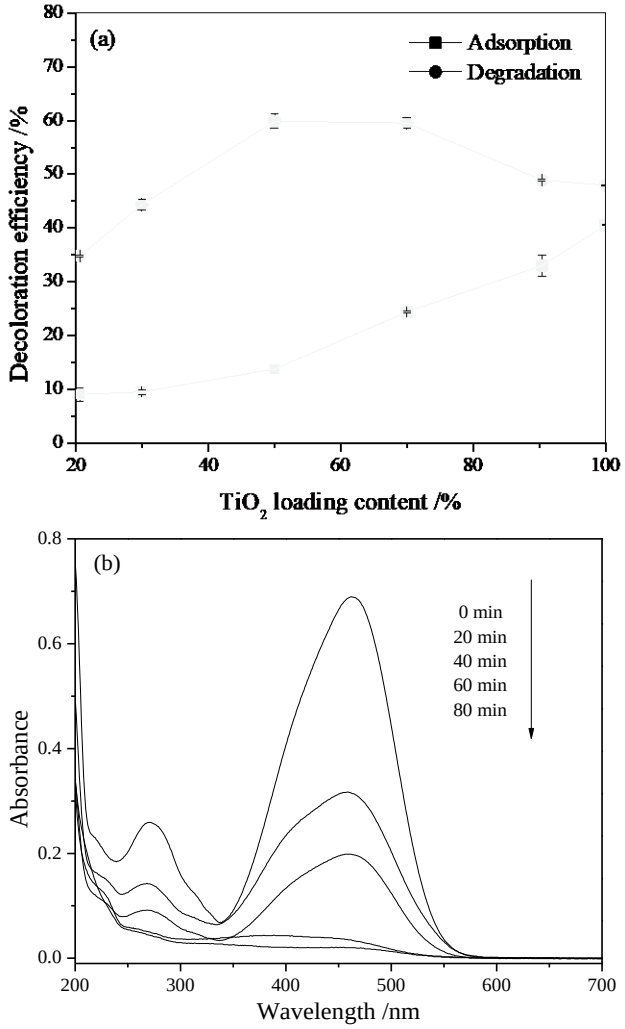


*Fig. 5. (a) Adsorption and photocatalytic degradation of methyl orange on In-$TiO_2$(x)/HZSM-5, (b) UV-Vis absorption spectra of methyl orange solution in presence of In-$TiO_2$(50%)/HZSM-5 during illumination*

## 4. Conclusions

The effects of In-$TiO_2$ loading content on the enhanced photocatalytic activity of In-$TiO_2$(*x*)/HZSM-5 photocatalyst were investigated. Anatase phase $TiO_2$ with the preferred orientation at the (101) plane is formed in the samples. In-$TiO_2$ is physically loaded on the surface of HZSM-5 particles. The bandgap energy is enlarged after supporting. Methyl orange molecules are almost decomposed after 80 min of irradiation on the In-$TiO_2$(50%)/HZSM-5.

## References

[1] D. Chatterjee, S. Dasgupta, J. Photochem. Photobiol. C **6**, 186 (2005).
[2] W. J. Zhang, Y. Li, F. H. Wang, J. Mater. Sci. Technol. **18**, 101 (2002).
[3] A. Fujishima, T. N. Rao, D. A. Tryk, J. Photoch. Photobio. C **1**, 1 (2000).
[4] W. J. Zhang, Z. Ma, K. X. Li, L. L. Yang, H. Li, H. B. He, Curr. Nanosci. **12**, 514 (2016).
[5] P. Zhou, J. H. Wu, W. L. Yu, G. H. Zhao, G. J. Fang, S. W. Cao, Appl. Surf. Sci. **319**, 167 (2014).
[6] S. M. López, M. C. Hidalgo, J. A. Navío, Appl. Catal. A **404**, 59 (2011).
[7] M. R. Hoffmann, S. T. Martin, W. Choi, W. Bahnemann, Chem. Rev. **95**, 69 (1995).
[8] G. Plantard, T. Janin, V. Goetz, S. Brosillon, Appl. Catal. B **115–116**, 38 (2012).
[9] H. J. Feng, M. H. Zhang, L. E. Yu, Appl. Catal. A **413–414**, 238 (2012).
[10] C. Han, J. Andersen, V. Likodimos, P. Falaras, J. Linkugel, D. D. Dionysiou, Catal. Today **224** 132 (2014).
[11] J. G. Yu, J. F. Xiong, B. Cheng, S. W. Liu, Appl. Catal. B **60**, 211 (2005).
[12] S. F. Chen, X. L. Yu, H. Y. Zhang, J. Hazar. Mater. **180**, 735 (2010).
[13] E. V. Skorb, E. A. Ustinovich, A. I. Kulak, J. Photoch. Photobio. A **193**, 97 (2008).
[14] M. A. O'Neill, F. L. Cozens, N. P. Schepp, J. Phys. Chem. B **105**, 12746 (2001).
[15] W. J. Zhang, Z. Ma, K. X. Li, L. L. Yang, H. Li, H. B. He, Curr. Nanosci. **12**, 514 (2016).
[16] W. J. Zhang, F. F. Bi, Y. Yu, H. B. He, J. Mole. Catal. A: Chem. **372**, 6 (2013).
[17] M. Takeuchi, T. Kimura, M. Hidaka, D. Rakhmawaty, M. Anpo, J. Catal. **246**, 235 (2007).
[18] V. Durgakumari, M. Subrahmanyama, K.V. Subba Rao, A. Ratnamala, M. Noorjahan, K. Tanaka, Appl. Catal. A **234**, 155 (2002).
[19] D. Dumitriu, R. Barjega, L. Frunza, J. Catal. **219**, 337 (2003).
[20] S. Narayanan, J. Judith, S. Sivasanker, Power Technol. **274**, 338 (2015).
[21] A. Tuel, Zeolites **16**, 108 (1996).
[22] N. Venkatachalam, M. Palanichamy, A. Banumathi, Catal. Comm. **8**, 1088 (2007).
[23] P. Kubelka, F. Z. Munk, Tech. Phys. **12**, 593 (1931).
[24] M. A. Butler, J. Appl. Phys. **48**, 1914 (1977).
[25] W. J. Zhang, J. L. Chen, H. B. He, J. Adv. Oxid. Technol. **17**, 365 (2014).

*Corresponding author: wjzhang@aliyun.com